

# Sustainable Use of Sugarcane Bagasse Ash in Fly Ash-based Geopolymers: Implications for Compressive Strength and Shrinkage

Thao-Van Vo<sup>1</sup>, Vu To-Anh Phan<sup>2</sup>, Duc-Hien Le<sup>2\*</sup>

<sup>1</sup> Faculty of Civil Engineering, Ton Duc Thang University, No. 19 Nguyen Huu Tho Street, 70000 Ho Chi Minh City, Vietnam

<sup>2</sup> Sustainable Developments in Civil Engineering Research Group, Faculty of Civil Engineering, Ton Duc Thang University, No. 19 Nguyen Huu Tho Street, 70000 Ho Chi Minh City, Vietnam

\* Corresponding author, e-mail: [leduchien@tdtu.edu.vn](mailto:leduchien@tdtu.edu.vn)

Received: 27 March 2025, Accepted: 19 May 2025, Published online: 05 June 2025

## Abstract

Geopolymers are synthesized through the reaction between alkaline activator solutions and aluminosilicate-rich precursors, offering an alternative to Portland cement for sustainable construction. Sugarcane bagasse ash (SCBA), an agricultural byproduct rich in  $\text{SiO}_2$ , presents potential for incorporation into fly ash (FA)-based geopolymer systems. While SCBA has been explored for environmental benefits, limited studies have evaluated the combined influence of SCBA and alkaline activator solutions on hardening behavior. This study investigated the effects of SCBA content (0%, 10%, 20%, 30% by mass), NaOH concentration (8M, 12M, 16M), and liquid-to-solid (L/S) ratio (0.2, 0.4, 0.6) using 36 geopolymer paste mixtures. SCBA was processed by drying, sieving to 149  $\mu\text{m}$ , and calcining at 700 °C for 2 hours. Specimens were cured at 90°C for 24 hours, followed by ambient curing. Bulk density, apparent porosity, water absorption, compressive strength, and shrinkage were evaluated. Results showed that SCBA content and L/S ratio strongly affected compressive strength and shrinkage. The mixture containing 10% SCBA, NaOH 12M, and L/S = 0.4 achieved the highest compressive strength (47.65 MPa at 90 days), along with reduced porosity and water absorption. In contrast, SCBA replacement above 20% resulted in decreased strength and increased shrinkage. The results indicate the potential of SCBA as a partial FA replacement to promote sustainable construction materials.

## Keywords

alkaline activation solution, NaOH concentration, L-to-S ratio, compressive strength, shrinkage

## 1 Introduction

Cement production is a major contributor to global carbon dioxide ( $\text{CO}_2$ ) emissions, accounting for approximately 8% of total anthropogenic  $\text{CO}_2$  emissions. These emissions primarily result from the energy-intensive calcination of limestone and the combustion of fossil fuels [1]. In 2022, the global cement industry produced approximately 4.1 billion metric tons [2]. Despite ongoing efforts to mitigate emissions through alternative fuels and clinker substitution, the industry's  $\text{CO}_2$  emissions remain above 2.5 billion metric tons annually. The high environmental burden of cement production has led to an increased focus on developing alternative binders [3].

Geopolymers are inorganic binders that were synthesized through the alkali activation of precursors such as fly ash (FA) [4]. Geopolymer materials exhibit high strength and durability due to the formation of stable three-dimensional polymer networks [5]. Unlike Portland

cement, geopolymer production does not require limestone calcination, leading to a significant reduction in  $\text{CO}_2$  emissions [6]. In addition to reducing carbon footprints, geopolymers enable the valorization of industrial by-products, thereby mitigating landfill waste and conserving natural resources [7]. Moreover, geopolymers exhibit superior resistance to acid and sulfate attack and demonstrate high thermal stability, making them viable alternatives to conventional cement for infrastructure [4].

Alkaline activator solutions have been identified as a primary factor influencing the dissolution of aluminosilicate precursors and the strength development of geopolymer materials [8, 9]. High concentration of NaOH solution increases the solubility of aluminosilicate materials, leading to improved strength [10]. However, NaOH with too high a concentration can reduce the workability and increase the brittleness [11]. Shee-Ween et al. [12] and

Vigneshkumar et al. [13] found that 14 M NaOH resulted in the highest compressive strength and lowest porosity, optimizing the geopolymer mechanical performance and microstructure. However, Ghafoor et al. [14] and Rajkumar [15] suggested that the optimum compressive strength, splitting tensile strength, and improved workability were achieved at 12 M. The alkaline activator solutions to solid ratio by mass (L/S) is also a strong factor influencing the properties of geopolymers [16]. Marczyk et al. found that low the L/S ratios generally increase strength but can lead to mixing challenges and L/S = 0.33 yields denser microstructures and improved flexural strength, while higher L/S ratios (0.45) lead to porous structures and reduced strength due to excessive water hindering geopolymer network formation [17]. However, Teng et al. suggested that L/S = 0.45 is the optimal ratio for the highest compressive strength and workability [18]. Besides, the  $\text{Na}_2\text{SiO}_3/\text{NaOH}$  ratio of 2.5 has been widely recognized as optimal for balancing strength development and workability [19].

The sugarcane industry generates approximately 1.9 billion metric tons of sugarcane annually [20]. Sugarcane bagasse ash (SCBA) is a byproduct produced in sugarcane industries during the autocombustion process in cogeneration boilers [20]. Improper disposal of SCBA contributes to environmental pollution [21]. SCBA contains silica ( $\text{SiO}_2$ ) and alumina ( $\text{Al}_2\text{O}_3$ ), making it a potential precursor for geopolymers [22]. Research has demonstrated the potential of SCBA, with its incorporation into geopolymer enhancing durability while supporting sustainable construction [20, 23]. Rihaan et al. suggested that geopolymer concrete achieved the highest strength when replacing 5% of FA mass with SCBA. However, at higher replacement levels (up to 20%), the strength and slump of the concrete decreased sharply [24]. Somna et al. found that replacing FA with SCBA at 10, 20, and 30% increased water absorption and decreased compressive strength values [25]. The addition of SCBA to FA geopolymers reduces compressive strength due to unreactive quartz in SCBA. However, up to 10 wt.% SCBA has minimal impact on properties, while higher amounts significantly decrease strength [26].

Previous research has highlighted the inconsistent effects of alkaline activator solutions on fly ash-based geopolymer [12–15], while SCBA is generally known to reduce the strength or workability of geopolymer materials [10, 25]. However, the combined influence of SCBA and alkaline activator solutions on the strength and shrinkage of fly ash-based geopolymer remains underexplored and warrants further investigation [24, 26]. Therefore, this study aims to assess the simultaneous impact of SCBA and Alkaline

activator solutions on the properties of fly ash-based geopolymer. To achieve this, experiments were conducted to evaluate bulk density, water absorption, apparent porosity, compressive strength, and shrinkage. Additionally, the density, the loss on ignition, microstructure, chemical composition, and mineral properties of SCBA were analyzed. The diagram of this study is illustrated in Fig. 1.

## 2 Materials and methods

### 2.1 Materials

The primary materials utilized in this investigation include sugarcane bagasse ash (SCBA), fly ash (FA) (class F, bulk density of  $1.56 \text{ g/cm}^3$  and specific gravity of  $2.71 \text{ g/cm}^3$ ), sodium hydroxide (pellets), sodium silicate solution ( $\text{Na}_2\text{SiO}_3$ ), and water.

The raw sugarcane bagasse ash was collected from a waste dump at a sugar mill in southern Vietnam. This agro-waste ash was produced after burning sugarcane bagasse in boilers at temperatures ranging from 500 to 600 °C for approximately 1.5 hours. Upon transportation to the laboratory, the raw SCBA was dried at 110 °C until a constant mass was achieved. The next treatment step was to sieve SCBA through a No. 100 sieve (149  $\mu\text{m}$ ) to remove large particles. Finally, the SCBA was calcined in a vacuum furnace with a maximum temperature of 700 °C (10 °C/min heating rate). After the vacuum furnace cooled to room temperature, the processed SCBA was stored in sealed plastic container. After processing, SCBA exhibited a gray color, a bulk density of  $0.73 \text{ g/cm}^3$ , and a specific gravity of  $2.12 \text{ g/cm}^3$ .

The alkaline solution consisted of sodium hydroxide solution (NaOH) and sodium silicate solution ( $\text{Na}_2\text{SiO}_3$ ): 9%  $\text{Na}_2\text{O}$  + 28%  $\text{SiO}_2$  + 63%  $\text{H}_2\text{O}$ , by mass. The preparation of the NaOH from sodium hydroxide (pellets) and tap water was carried out 24 hours before mixing the geopolymer mixtures.

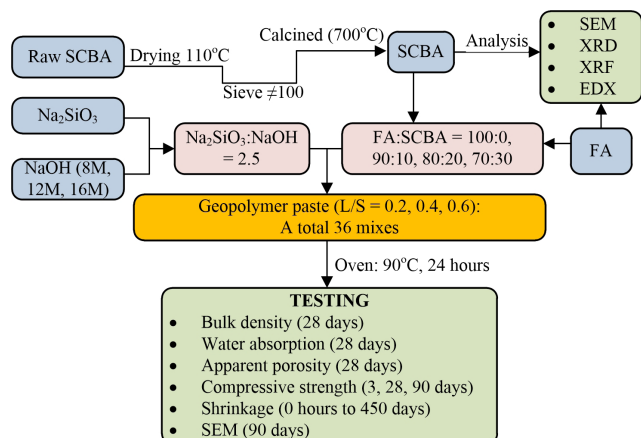


Fig. 1 The diagram in this study

## 2.2 Mix proportions

Table 1 displays the mix proportions of 36 geopolymer paste mixtures in this study. Four mass percentages of sugarcane bagasse ash (SCBA) replacing fly ash (FA) in the mixture (i.e., 0%, 10%, 20%, and 30%) were proposed to form four groups of mixtures named A, B, C, and D, respectively. The molarity of NaOH was 8M, 12M, and 16M. The mass ratio between  $\text{Na}_2\text{SiO}_3$  and NaOH was maintained at 2.5. The L/S ratios were established at 0.2, 0.4, and 0.6.

## 2.3 Sample preparation and curing

The preparation of the geopolymer mixture was conducted in five sequential steps. In the first step, fly ash (FA) and sugarcane bagasse ash (SCBA) were dry-mixed in a high-shear mixer for 3 minutes. In the second step, NaOH was stirred and gradually added to the dry mixture, followed by continuous mixing for an additional 3 minutes. In the third step,  $\text{Na}_2\text{SiO}_3$  was stirred and slowly introduced into the mixture, which was then mixed for

**Table 1** Mix proportion (1000 grams of geopolymer paste mixture)

No	Group	Mix ID	FA	SCBA	NaOH	$\text{Na}_2\text{SiO}_3$	FA/SCBA	L/S
1	A	A-0.2-8	833	0	48 (8M)	119	100/0	0.2
2		A-0.4-8	714	0	82 (8M)	204	100/0	0.4
3		A-0.6-8	625	0	107 (8M)	268	100/0	0.6
4		A-0.2-12	833	0	48 (12M)	119	100/0	0.2
5		A-0.4-12	714	0	82 (12M)	204	100/0	0.4
6		A-0.6-12	625	0	107 (12M)	268	100/0	0.6
7		A-0.2-16	833	0	48 (16M)	119	100/0	0.2
8		A-0.4-16	714	0	82 (16M)	204	100/0	0.4
9		A-0.6-16	625	0	107 (16M)	268	100/0	0.6
10	B	B-0.2-8	750	83	48 (8M)	119	90/10	0.2
11		B-0.4-8	643	71	82 (8M)	204	90/10	0.4
12		B-0.6-8	563	63	107 (8M)	268	90/10	0.6
13		B-0.2-12	750	83	48 (12M)	119	90/10	0.2
14		B-0.4-12	643	71	82 (12M)	204	90/10	0.4
15		B-0.6-12	563	63	107 (12M)	268	90/10	0.6
16		B-0.2-16	750	83	48 (16M)	119	90/10	0.2
17		B-0.4-16	643	71	82 (16M)	204	90/10	0.4
18		B-0.6-16	563	63	107 (16M)	268	90/10	0.6
19	C	C-0.2-8	667	167	48 (8M)	119	80/20	0.2
20		C-0.4-8	571	143	82 (8M)	204	80/20	0.4
21		C-0.6-8	500	125	107 (8M)	268	80/20	0.6
22		C-0.2-12	667	167	48 (12M)	119	80/20	0.2
23		C-0.4-12	571	143	82 (12M)	204	80/20	0.4
24		C-0.6-12	500	125	107 (12M)	268	80/20	0.6
25		C-0.2-16	667	167	48 (16M)	119	80/20	0.2
26		C-0.4-16	571	143	82 (16M)	204	80/20	0.4
27		C-0.6-16	500	125	107 (16M)	268	80/20	0.6
28	D	D-0.2-8	667	167	48 (8M)	119	70/30	0.2
29		D-0.4-8	571	143	82 (8M)	204	70/30	0.4
30		D-0.6-8	500	125	107 (8M)	268	70/30	0.6
31		D-0.2-12	667	167	48 (12M)	119	70/30	0.2
32		D-0.4-12	571	143	82 (12M)	204	70/30	0.4
33		D-0.6-12	500	125	107 (12M)	268	70/30	0.6
34		D-0.2-16	667	167	48 (16M)	119	70/30	0.2
35		D-0.4-16	571	143	82 (16M)	204	70/30	0.4
36		D-0.6-16	500	125	107 (16M)	268	70/30	0.6

a further 5 minutes. During all three mixing steps, the impeller speed of the mixer was maintained at a constant 140 (rpm). In the fourth step, the prepared geopolymer mixture is poured into the mold in 5 equal layers. Before that, the mold has been coated with a thin layer of beef fat to prevent sticking. Finally, the molds were placed on a vibrating table with an amplitude of 0.85 mm/0.75 mm and a frequency of 50 Hz for 2 minutes. After vibration, the sample surface was flattened with a glass plate. Cube molds with dimensions of 50 mm were used for testing bulk density, water absorption, apparent porosity, and compressive strength. Prismatic molds measuring 25 × 25 × 285 mm were utilized to measure shrinkage.

The curing process was initiated immediately after casting. The molds were wrapped with a thin plastic film to prevent moisture loss and placed in an oven set at 90 °C for 24 hours. After drying, the oven was turned off and allowed to cool gradually to room temperature (approximately 12 hours) while the molds remained inside to prevent sudden temperature changes. After cooling, the molds were removed from the oven, and the samples were demolded from the molds. Finally, specimens were placed on a flat, non-absorbent surface and were cured at room temperature (25 ± 2 °C and 80 ± 4% relative humidity (RH)). The age of the sample was determined from the time the sample was removed from the molds (T<sub>0</sub>). Fig. 2 shows the diagram of preparation and curing specimens.

### 2.4 Testing methods

All testing items and corresponding ASTM standards for specimens in this study were encapsulated in Table 2.

Bulk density, water absorption, and apparent porosity of geopolymer samples were determined following ASTM C642-21 [27]. Three samples (28 days of age) were tested for each geopolymer material, and the average value was recorded. Initially, the specimens were dried in an oven at 105 ± 5 °C until a constant mass. The dry mass (A) was recorded using an electronic balance (±0.1 g accuracy).

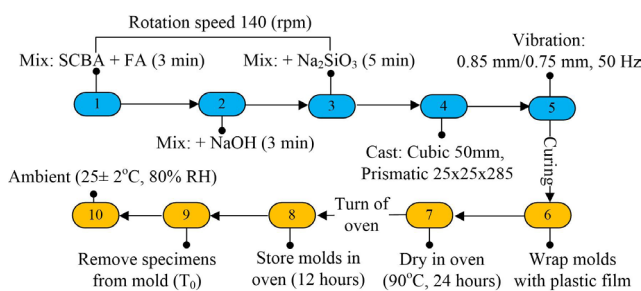


Fig. 2 Diagram of making and curing specimens

Table 2 Testing items, size, and number of specimens

Testing items	Testing methods	Size (mm)/number of specimens	Testing ages
Bulk density			
Water absorption	ASTM C642-21	50 × 50 × 50 (36 × 3 = 180)	28 days
Apparent porosity			
Compressive strength	ASTM C109/C109M-20	50 × 50 × 50 (36 × 3 × 3 = 324)	3, 28, 90 days
Shrinkage	ASTM C596-23	25 × 25 × 285 (8 × 2 = 16)	0, 3, 6, 12, 24 hours, and 3, 7, 14, 28, 56, 112, 182, 27, 360, 450 days

Subsequently, the samples were allowed to cool to room temperature before further testing. Next, the specimens were immersed in water at room temperature for 48 hours. After removal, the specimens were surface-dried with a damp cloth, and the saturated surface-dry mass (B) was recorded. Finally, the submerged mass (C) was measured using a suspended balance while the specimens were fully immersed in water. The bulk density (D), water absorption (W), and apparent porosity (P) were determined using Eqs. (1) to (3), respectively:

$$D(g/cm^3) = \frac{A}{B - C} \quad (1)$$

$$W(\%) = \frac{B - A}{A} \times 100 \quad (2)$$

$$P(\%) = \frac{B - A}{B - C} \times 100 \quad (3)$$

Compressive strength tests were conducted at 3, 28, and 90 days. The tests followed ASTM C109/C109M-20 [28]. A hydraulic compression machine with a maximum load capacity of 300 kN was used. The loading rate was set at 1000 N/s. The compressive strength was reported as the average of three specimens tested at each age.

The shrinkage of the samples measured included autogenous shrinkage, drying shrinkage, and carbonation shrinkage. The shrinkage test was referenced to ASTM C596-23 [29] and was conducted by a shrinkage measuring device (0.001 mm accuracy) at room temperature (25 ± 2 °C and 80 ± 4% RH). Eight geopolymer mixtures were tested, categorized based on variations in SCBA (A-0.4-12, B-0.4-12, C-0.4-12, D-0.4-12), NaOH concentration (B-0.4-8, B-0.4-12, B-0.4-16), and liquid-to-solid (L/S) ratios (B-0.2-12, B-0.4-12, B-0.6-12).

The initial specimen length ( $L_0$ ) was recorded at  $T_0$ , with subsequent measurements ( $L_i$ ) taken at 3 hours, 6 hours, 12 hours, 24 hours, and 3, 7, 14, 28, 56, 112, 182, 272, 360, and 450 days. Shrinkage values were reported as the average of two specimens measured at each designated time interval. Shrinkage was calculated using Eq. (4).

$$\text{Shrinkage (mm / m)} = \frac{L_i - L_0}{L_0} \times 1000. \quad (4)$$

### 3 Results and discussion

#### 3.1 Characterization of FA and SCBA

##### 3.1.1 Oxide composition

The chemical composition of fly ash (FA) and sugarcane bagasse ash (SCBA) was analyzed using X-ray fluorescence (XRF) spectroscopy. XRF analysis was performed using an S2 PUMA Series 2 XRF spectrometer (Germany), and data were processed using SPECTRA.ELEMENTS software [30]. Table 3 presents the main oxide compositions of fly ash (FA) and SCBA. FA primarily contained 56.15%  $\text{SiO}_2$ , 20.48%  $\text{Al}_2\text{O}_3$ , and 12.67%  $\text{Fe}_2\text{O}_3$ , along with smaller amounts of CaO,  $\text{K}_2\text{O}$ , MgO, and  $\text{P}_2\text{O}_5$ . The loss on ignition of FA, determined according to ACI 116, was 1.33%, measured by heating the sample to 900-1000 °C and recording the mass loss [31]. SCBA exhibited a higher  $\text{SiO}_2$  content (85.93%), with lower amounts of  $\text{Al}_2\text{O}_3$  (1.97%) and  $\text{Fe}_2\text{O}_3$  (1.18%). Minor oxides included CaO,  $\text{K}_2\text{O}$ , MgO, and  $\text{P}_2\text{O}_5$ . The loss on ignition of SCBA was recorded as 4.72%, following ACI 116 [31]. According to ASTM C618-22, both FA and SCBA are Class F pozzolans when  $\text{SiO}_2 > 50\%$ ,  $(\text{SiO}_2 + \text{Fe}_2\text{O}_3 + \text{Al}_2\text{O}_3) > 70\%$ , and the LOI  $< 6\%$  [32].

##### 3.1.2 X-ray diffraction results

The X-ray diffraction (XRD) analysis was performed using an X'PERT PRO diffractometer (PANalytical, United Kingdom) at 40 kV, 30 mA, and a scanning speed of 0.02 °/min. Fig. 3 presents the XRD patterns of fly ash (FA) and Sugarcane bagasse ash (SCBA). The XRD analysis of FA identified distinct peaks corresponding to quartz, mullite, and hematite. Additionally, a broad hump between 20° and 35° (2 $\theta$ ) indicates the presence of an amorphous phase. SCBA exhibits strong quartz and cristobalite peaks, indicating a high crystal phase.

**Table 3** Oxide compositions of FA and SCBA (% by mass)

Oxide	$\text{SiO}_2$	$\text{Al}_2\text{O}_3$	$\text{Fe}_2\text{O}_3$	CaO	$\text{K}_2\text{O}$	MgO	LOI (%)
FA	56.15	20.48	12.67	4.33	1.05	0.95	1.33
SCBA	85.93	1.97	1.18	1.21	1.25	3.63	4.72

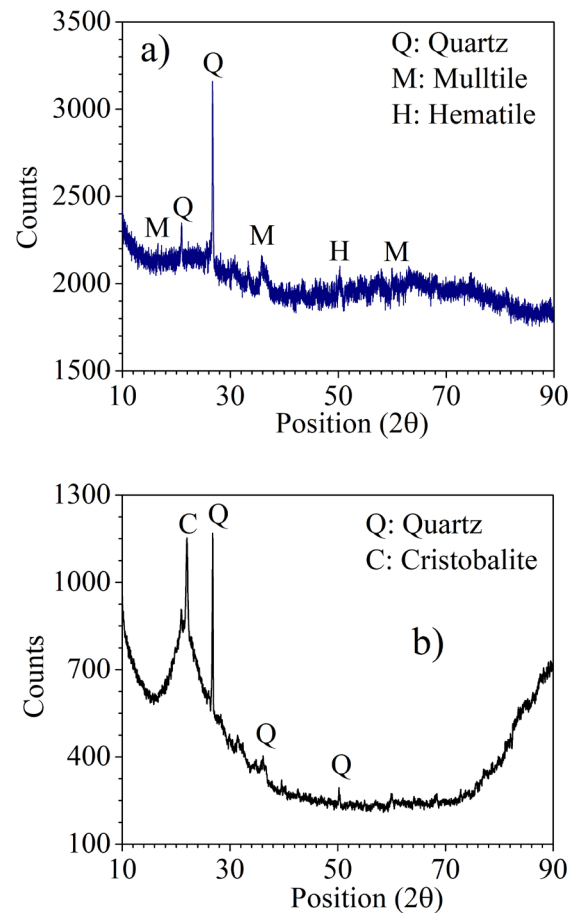


**Fig. 3** X-ray diffraction (XRD) pattern, (a) FA, (b) SCBA

##### 3.1.3 Scanning electron microscopy and Energy-dispersive X-ray spectroscopy

The morphology of fly ash (FA) and sugarcane bagasse ash (SCBA) was analyzed using scanning electron microscopy (SEM). SEM imaging was conducted using a Hitachi S-4800 FESEM (Japan) at 10 kV to observe particle shape and size. SEM images of FA (Fig. 4(a)) revealed smooth, spherical particles with sizes commonly ranging from ~1  $\mu\text{m}$  to 5  $\mu\text{m}$ . SEM imaging of SCBA (Fig. 4(b)) displayed irregular, angular particles with a porous structure, with sizes ranging from ~1  $\mu\text{m}$  to 13  $\mu\text{m}$ .

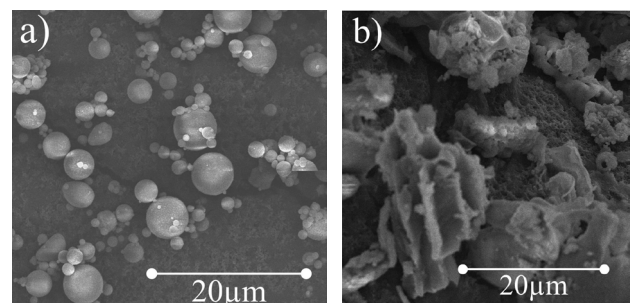


**Fig. 4** Micrographs, (a) SEM of FA, (b) SEM of SCBA

The elemental composition of FA and SCBA was analyzed using energy-dispersive X-ray spectroscopy (EDX) by the EDX H-7593 Horiba (UK) system, integrated with EMAX-Analyser software to identify the main elements in the samples [33]. Silicon (Si), aluminum (Al), iron (Fe), calcium (Ca), and oxygen (O) were found in FA's EDX spectrum (Fig. 5(a)). The EDX spectrum of SCBA (Fig. 5(b)) showed that silicon (Si), aluminum (Al), oxygen (O), and carbon (C) were present. A distinct carbon (C) peak was observed in the SCBA spectrum.

### 3.2 Hardening properties geopolymer materials

Table 4 summarizes the hardening properties of 36 geopolymer samples with varying sugarcane bagasse ash (SCBA) levels, NaOH concentrations, and L/S ratios. The general trend shows that as the SCBA ratio increases, bulk density tends to decrease, while apparent porosity and water absorption increase. Specifically, the sample with the highest bulk density is A-0.4-12 (2.18 g/cm<sup>3</sup>), while the lowest value belongs to D-0.2-8 (1.49 g/cm<sup>3</sup>). Apparent porosity reaches its highest value at D-0.2-8 (19.90%) and the

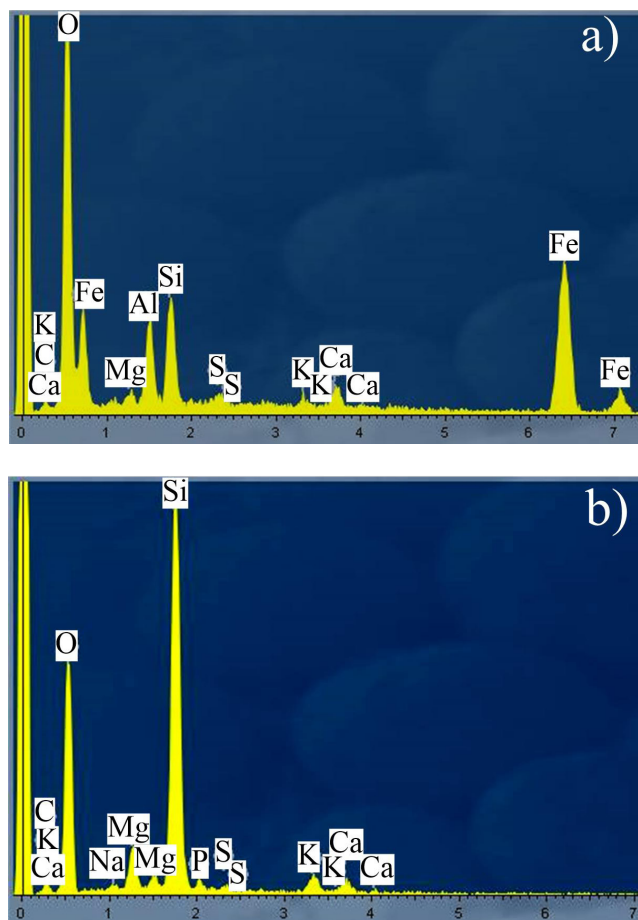


Fig. 5 Micrographs, (a) EDX of FA, (b) EDX of SCBA

lowest at B-0.4-12 (4.78%). Water absorption ranges from 2.12% (B-0.4-12, lowest) to 10.63% (D-0.2-8, highest).

Compressive strength varies significantly among samples. The highest value after 90 days is recorded for B-0.4-12 (47.65 MPa), while the lowest is observed in D-0.2-8 (9.87 MPa). Samples with SCBA replacement of 20% and 30% tend to show a significant reduction in compressive strength. Alkali concentration and L/S ratio strongly influence the properties of geopolymer. Using an NaOH concentration of 12M and an L/S ratio of 0.4 usually results in the highest compressive strength.

#### 3.2.1 Effect of SCBA on bulk density, apparent porosity and water absorption

Fig. 6 shows significant variations in bulk density, apparent porosity, and water absorption as sugarcane bagasse ash (SCBA) content increases. Bulk density decreases steadily with SCBA replacement. At 10% replacement, the reduction is minor; at 20%, the decrease exceeds 10% compared to the control group; and at 30%, the reduction reaches over 18%. In contrast, apparent porosity increases markedly. When SCBA content rises from 10% to 30%, apparent porosity nearly doubles. The lowest apparent porosity is observed in B-0.4-12 (6.78%) and the highest in D-0.2-8 (13.72%). Water absorption increases in parallel with porosity. At 10% SCBA, the increase is negligible, but at 20%, absorption reaches 1.8 times that of Group A, and at 30%, it is approximately 2.3 times higher. The sample B-0.4-12 shows the lowest water absorption (3.15%), and D-0.2-8 the highest (7.09%).

The decline in bulk density corresponds to the low density, high porosity, and irregular morphology of SCBA particles, which disrupt particle packing in the geopolymer matrix [20, 22]. Crystalline quartz and cristobalite in SCBA exhibit low reactivity, impeding geopolymerization [23], while high the loss on ignition reduces mixture uniformity [24].

This trend aligns with Rihan et al. [21], who reported lower density and increased porosity at 20-30% SCBA. França et al. [23] found that higher SCBA increased water absorption. In contrast, Somna et al. [25] observed minimal adverse effects at 10% SCBA, consistent with the dense structure in Group B of the current study.

#### 3.2.2 Effect of NaOH concentration and L/S ratio on bulk density

Fig. 7 presents the variation in bulk density of geopolymer materials under different NaOH concentrations and

**Table 4** Hardening properties of geopolymer materials

No	Mix ID	D (g/cm <sup>3</sup> )	W (%)	P (%)	Compressive strength (MPa)		
					3 days	28 days	90 days
1	A-0.2-8	2.06	5.12	10.47	19.27	25.14	25.93
2	A-0.4-8	2.15	4.27	8.95	33.86	40.73	41.64
3	A-0.6-8	2.13	4.2	9.03	33.34	38.21	39.24
4	A-0.2-12	2.11	4.66	9.95	28.74	35.33	37.01
5	A-0.4-12	2.18	3.98	8.69	36.87	45.65	47.28
6	A-0.6-12	2.14	3.73	8.84	37.45	42.85	43.57
7	A-0.2-16	2.07	4.78	10.02	28.87	35.75	37.17
8	A-0.4-16	2.17	4.06	8.93	36.41	43.20	45.17
9	A-0.6-16	2.12	3.81	8.92	33.12	41.32	41.80
10	B-0.2-8	1.94	4.83	9.11	12.66	17.41	18.76
11	B-0.4-8	2.12	3.05	6.93	31.19	42.99	46.37
12	B-0.6-8	2.11	2.91	6.26	29.43	40.21	43.27
13	B-0.2-12	2.10	3.81	8.05	20.85	26.43	28.49
14	B-0.4-12	2.15	2.12	4.78	34.32	44.50	47.65
15	B-0.6-12	2.12	2.24	5.27	33.91	43.61	45.50
16	B-0.2-16	2.00	3.93	8.13	18.13	24.14	24.80
17	B-0.4-16	2.06	2.85	6.46	32.89	44.47	47.47
18	B-0.6-16	2.05	2.57	6.01	28.69	37.85	40.79
19	C-0.2-8	1.78	8.25	15.11	9.94	14.11	15.73
20	C-0.4-8	1.98	6.73	12.73	22.16	30.84	34.49
21	C-0.6-8	1.96	5.55	10.88	22.76	31.60	34.75
22	C-0.2-12	1.92	6.18	12.05	14.48	19.45	21.98
23	C-0.4-12	2.09	5.17	9.89	26.52	36.51	40.60
24	C-0.6-12	2.05	4.43	9.15	28.65	37.71	42.41
25	C-0.2-16	1.94	5.65	11.02	14.49	21.46	23.25
26	C-0.4-16	2.08	4.62	9.19	28.00	38.81	41.53
27	C-0.6-16	2.07	4.19	8.52	29.11	39.48	42.01
28	D-0.2-8	1.49	10.63	19.90	5.89	8.60	9.87
29	D-0.4-8	1.63	7.96	14.81	18.16	26.01	30.24
30	D-0.6-8	1.84	7.15	13.72	18.21	27.10	31.46
31	D-0.2-12	1.55	7.09	13.66	8.52	13.11	15.12
32	D-0.4-12	1.80	6.27	12.74	21.78	32.44	36.48
33	D-0.6-12	1.89	6.11	11.98	23.18	35.10	38.57
34	D-0.2-16	1.57	6.91	13.33	9.14	13.43	16.75
35	D-0.4-16	1.82	5.88	11.85	23.16	32.30	38.34
36	D-0.6-16	1.91	5.85	11.52	26.13	37.30	41.28

liquid-to-solid (L/S) ratios across four sugarcane bagasse ash (SCBA) groups. An increase in NaOH concentration from 8M to 12M leads to a rise in bulk density in all groups. Groups A and B show increases of 2-5%, followed by a slight reduction at 16M. Group C experiences an increase of approximately 5-6%, maintaining stability at 16M. Group D exhibits a continuous increase up to 16M, resulting in a total gain of around 12%. An increase in L/S

ratio from 0.2 to 0.4 results in a bulk density improvement ranging from 3% to 7%, depending on SCBA content. At L/S = 0.6, a minor decrease of 1-2% occurs in Groups A and B, while Groups C and D show an increase of 3-4%. The highest bulk density is consistently observed at L/S = 0.4. At L/S = 0.6, the effect of NaOH concentration becomes less pronounced (< 4%).

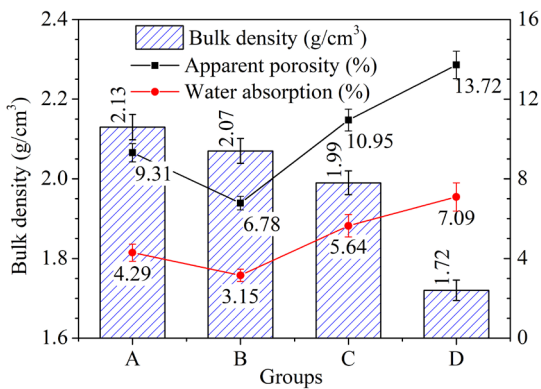


Fig. 6 Effect of SCBA on bulk density, apparent porosity, and water absorption

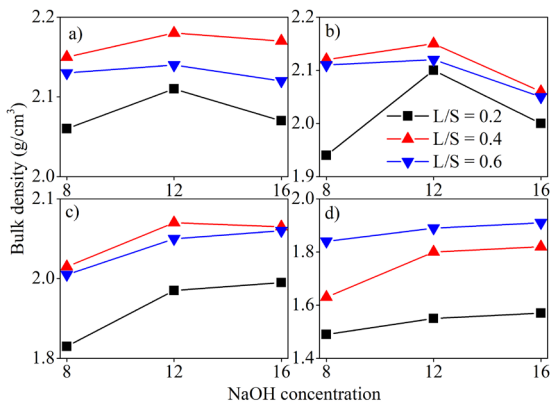


Fig. 7 Effect of NaOH concentration and L/S ratio on bulk density, (a) Group A, (b) Group B, (c) Group C, (d) Group D

The increase in bulk density from 8M to 12M NaOH can be attributed to enhanced dissolution of aluminosilicate species, forming a denser and more continuous geopolymer gel structure [12]. However, at 16M, the excess sodium ions may react with atmospheric CO<sub>2</sub> to form sodium carbonate, leading to microstructural disruption and a slight reduction in bulk density, especially in Groups A and B with low SCBA content [14]. At L/S = 0.4, the highest bulk density (2.18 g/cm<sup>3</sup> in A-0.4-12) were observed. At L/S = 0.6, excessive liquid causes poor packing efficiency and increases inter-particle spacing, resulting in lower density - an effect confirmed in the study of Aliabdo et al. [19].

In high-SCBA systems (Group D), the porous structure of SCBA enhances alkali absorption and retains more of the activator solution within the matrix. This behavior minimizes negative effects of alkali saturation, allowing continuous bulk density increase up to 16M, consistent with results reported by Rihan et al. [24]. Additionally, reduced sensitivity to L/S and NaOH concentration at SCBA levels above 20% has been associated with altered particle morphology and decreased gel phase formation due to crystalline content [25].

### 3.2.3 Effect of NaOH concentration and L/S ratio on apparent porosity

Fig. 8 illustrates the variation in apparent porosity of geopolymer materials across different sugarcane bagasse ash (SCBA) contents as influenced by NaOH concentration and L/S ratio. In Groups A and B (0% and 10% SCBA), porosity decreased as NaOH increased from 8M to 12M, followed by a slight rise at 16M. Specifically, Group A showed a reduction from 10.47% to 9.95%, then increased to 10.02%. Group B decreased from 9.11% to 8.05%, then increased to 8.13%. Conversely, Groups C and D (20% and 30% SCBA) exhibited continuous porosity reduction with increasing NaOH. In Group C, porosity decreased from 15.11% to 11.02%, while Group D decreased from 19.90% to 13.33%. The L/S ratio of 0.4 resulted in the lowest porosity values in Groups A-C, while 0.6 yielded the minimum in Group D.

The decline in porosity with increasing NaOH concentration is attributed to enhanced dissolution of aluminosilicate phases, promoting gel formation and matrix densification [12, 13]. However, at 16M, excess Na<sup>+</sup> ions may result in sodium carbonate precipitation, which interrupts gel continuity and creates microstructural voids in systems with low SCBA content [14, 23]. At higher SCBA levels, the porous surface area and residual carbon content enhance alkali uptake and prolong the reaction, thus maintaining structural compactness [24]. Microstructural observations confirm denser matrix development when SCBA content exceeds 20%, particularly at 16M NaOH [21, 24]

The L/S ratio also plays a crucial role in porosity development. A ratio of 0.4 provides a sufficient solution for precursor activation without leaving excess liquid, which otherwise contributes to pore formation [17]. At 0.6, porosity increases in Groups A and B due to poor particle packing and excessive voids. In contrast,

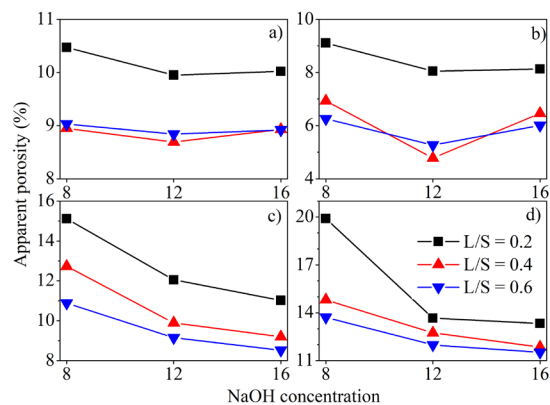


Fig. 8 Effect of NaOH concentration and L/S ratio Apparent porosity, (a) Group A, (b) Group B, (c) Group C, (d) Group D

Groups C and D exhibit further porosity reduction, suggesting that SCBA improves internal liquid distribution and gel connectivity at higher L/S values [25]. This trend aligns with results from Teng et al. [18], where L/S optimization reduced porosity in fly ash systems, and with findings by França et al. [23], who confirmed that SCBA enhances gel stability and structural cohesion when used in combination with strong alkali activators.

### 3.2.4 Effect of NaOH concentration and L/S ratio on water absorption

Fig. 9 presents the influence of NaOH concentration and liquid-to-solid (L/S) ratio on the water absorption of geopolymer materials across varying SCBA contents. In Groups A and B (0–10% SCBA), water absorption decreases as NaOH increases from 8M to 12M, followed by a slight increase at 16M. Specifically, Group A shows a reduction from 5.12% to 4.66%, then a rise to 4.78%, while Group B decreases from 4.83% to 3.81%, increasing slightly to 3.93%. In contrast, Groups C and D (20–30% SCBA) exhibit continuous reductions across the range, from 8.25% to 5.65% in Group C and from 10.63% to 6.91% in Group D, with the lowest values observed at NaOH = 16M and L/S = 0.6.

The general decline in water absorption with increasing NaOH concentration is attributed to improved aluminosilicate dissolution and geopolymer gel formation, leading to fewer capillary pores and reduced water ingress [11, 19]. The slight increase at 16M in Groups A and B suggests that excessive alkali may hinder network development due to sodium carbonate precipitation, reducing matrix cohesion [23]. In contrast, in high-SCBA systems, water absorption continues to decline at 16M, which may result from the porous structure of SCBA enhancing alkali uptake and promoting extended gel formation [24, 25].

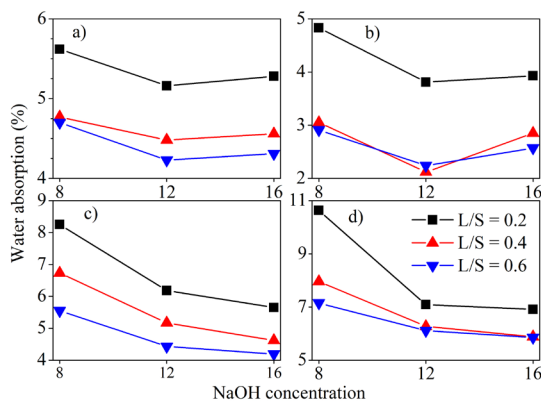


Fig. 9 Effect of NaOH concentration and L/S ratio water absorption, (a) Group A, (b) Group B, (c) Group C, (d) Group D

The L/S ratio significantly affects water absorption. A value of 0.4 leads to the lowest absorption due to balanced liquid distribution and optimal solid-phase activation [17, 19]. At L/S = 0.6, water absorption decreases further in Groups C and D, likely due to SCBA assisting in liquid retention and structural refinement. In Groups A and B, the benefit is less pronounced, possibly because excess liquid impedes compactness and increases porosity [19].

These findings align with observations by Teng et al. [18] and Marczyk et al. [17], which confirm that strong alkali activation combined with SCBA incorporation enhances microstructural density and reduces water permeability in geopolymer systems.

## 3.3 Compressive strength

### 3.3.1 Effect of SCBA on compressive strength

Fig. 10 presents the effect of sugarcane bagasse ash (SCBA) content on compressive strength in fly ash-based geopolymer paste. Compressive strength decreases progressively as SCBA replacement increases. At 10%, 20%, and 30% replacement levels, the reductions are approximately 9%, 23%, and 36%, respectively, compared to the control sample, indicating a strong influence of SCBA on compressive strength.

The decline in compressive strength with increasing SCBA is associated with its lower pozzolanic reactivity compared to fly ash, resulting in reduced formation of geopolymeric gels [10]. Although SCBA can participate in the geopolymerization process, excessive amounts introduce unreactive crystalline phases and increase porosity due to incomplete reaction, leading to strength reduction [11, 20]. SCBA contains low  $Al_2O_3$  content (Table 3), which limits the formation of cross-linked Si–O–Al bonds essential for mechanical strength development [21, 22, 34]. Additionally, high contents of quartz and cristobalite

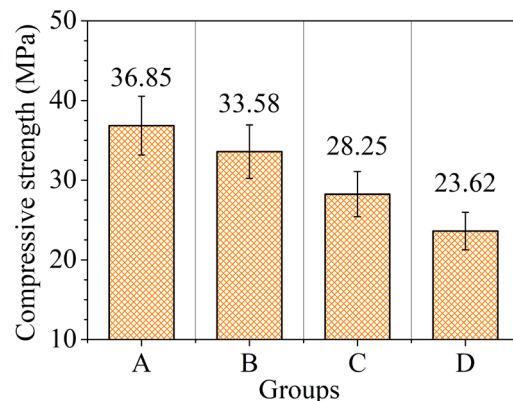


Fig. 10 Effect of SCBA on compressive strength

in SCBA (confirmed by XRD) exhibit low solubility in alkaline media, impeding geopolymer gel formation [20, 23]. Unburned carbon and high the loss on ignition further hinder matrix densification and disrupt the setting process, especially at high replacement levels [11, 21, 25].

Several studies support these findings. Rihan et al. [21] reported that above 20% SCBA, mechanical properties decreased significantly due to poor particle packing and delayed geopolymerization. Ahmad et al. [22] and França et al. [23] indicated that while SCBA may improve strength through a filler effect at low levels, excessive incorporation deteriorates bonding and densification. Somna et al. [25] observed a similar 9-10% reduction in compressive strength at 10% SCBA and a 20-25% drop at 20%, consistent with current results. However, at 30% SCBA, the observed strength was 5-7% lower than in previous reports, possibly due to variations in curing conditions and activator concentration.

### 3.3.2 Compressive strength and curing time

Fig. 11 illustrates the development of compressive strength at 3 and 90 days relative to 28-day strength ( $R_3/R_{28}$  and  $R_{90}/R_{28}$ ) across varying sugarcane bagasse ash (SCBA) contents. At 3 days, strength ratios decrease with increasing SCBA: 0.83 (0%), 0.75 (10%), 0.73 (20%), and 0.68 (30%). At 90 days, the trend reverses, with  $R_{90}/R_{28}$  values increasing to 1.07, 1.10, and 1.15 in Groups B, C, and D, while the control reaches 1.03.

Early strength reduction results from the slow dissolution of crystalline phases such as quartz and cristobalite present in SCBA, which delays gel formation [11, 20, 23]. Additionally, high loss on ignition (LOI) and residual carbon content obstruct initial geopolymerization by interfering with bond formation and promoting porosity [21, 22]. Over extended curing periods, gradual dissolution of reactive silica

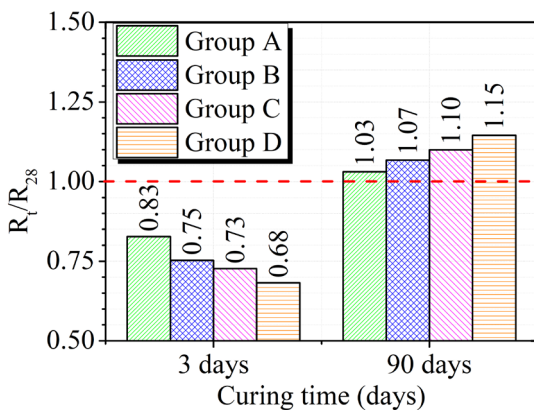


Fig. 11 Compressive strength and curing time

and alumina from SCBA enhances polycondensation, leading to matrix densification and late strength gain [23, 25].

This delayed strength development aligns with previous findings. Abdalla et al. [10] and Somna et al. [25] reported 20-30% and 10-20% long-term strength improvements, respectively, in SCBA-based geopolymers. Le et al. [20] and Rihan et al. [21] also confirmed that extended curing allows SCBA to actively participate in gel formation, compensating for initial reactivity limitations.

### 3.3.3 Effect of NaOH concentration and L/S ratio on compressive strength

Fig. 12 illustrates the influence of NaOH concentration and L/S ratio on compressive strength across all sugarcane bagasse ash (SCBA) groups. At 8M NaOH, the lowest compressive strength was recorded in all groups, with strength reductions ranging from 32.7% to 49.6% compared to peak values. The lowest strength was 8.12 MPa (Group D, L/S = 0.2). Increasing NaOH concentration from 8M to 12M resulted in strength gains of 42.2% (Group A), 43.7% (Group B), 40.6% (Group C), and 51.0% (Group D). Beyond 12M, compressive strength declined slightly in Groups A and B (4.6% and 3.1%) but increased in Groups C and D (2.2% and 3.1%).

L/S = 0.2 consistently resulted in the lowest strength across all groups, with reductions of 49.3% to 76.7%. Strength increased substantially when L/S rose to 0.4, improving by 65.1% (Group A), 83.5% (Group B), 75.5% (Group C), and 89.8% (Group D). A slight increase from L/S = 0.4 to 0.6 was only observed in Groups C and D (3.2% and 4.1%).

NaOH concentration strongly affects the dissolution of aluminosilicate precursors. Significant strength gains between 8M and 12M NaOH confirm improved geopolymerization, as also noted by Shee-Ween et al. [12] and Ghafoor et al. [14]. However, excessive alkali (16M) may cause

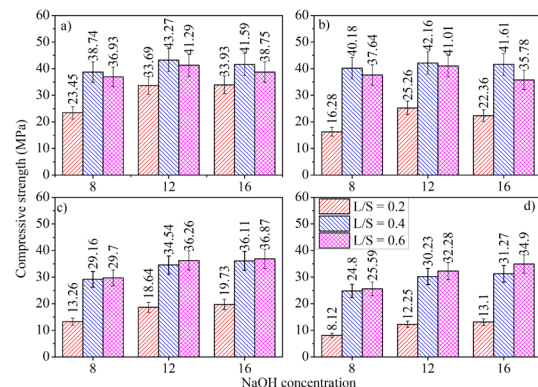


Fig. 12 Effect of NaOH concentration and L/S ratio on compressive strength, (a) Group A, (b) Group B, (c) Group C, (d) Group D

alkali precipitation or pore formation, weakening the matrix, consistent with findings from Vigneshkumar et al. [13] and Fernández-Jiménez et al. [16] In high-SCBA groups, continued strength gain at 16M indicates improved activation of quartz-rich SCBA under stronger alkali conditions [23].

Inadequate liquid at  $L/S = 0.2$  limits precursor dissolution, reducing strength [19].  $L/S = 0.4$  provided the most favorable condition, in agreement with Teng et al. [18] and Marczyk et al. [17]. At  $L/S = 0.6$ , the decline in low-SCBA groups agrees with Siyal [35], where excess liquid increased porosity. In contrast, SCBA-rich mixtures continued to improve due to higher fluid absorption capacity and slower reaction kinetics requiring extended availability of activator [21, 24].

Compared with low-reactive fly ash systems, SCBA-based geopolymers exhibit delayed but sustained activation. Rihan et al. [24] and França et al. [23] highlighted that higher NaOH and  $L/S$  ratios are essential for optimal SCBA utilization. These findings support the continued strength increase observed in Groups C and D under aggressive alkaline conditions.

### 3.4 Shrinkage

#### 3.4.1 Effect of SCBA on shrinkage

Fig. 13 illustrates the effect of sugarcane bagasse ash (SCBA) content on shrinkage in geopolymer paste over 450 days. A logarithmic time scale was used to highlight long-term behavior. In the early stage (1-100 hours), all groups exhibited rapid shrinkage, primarily due to initial water loss. However, the shrinkage rate varied with SCBA content. Groups A and B (0% and 10% SCBA) stabilized earlier, with final shrinkage values of 1.49 mm/m and 2.46 mm/m, respectively. In contrast, Groups C and D (20% and 30% SCBA) continued shrinking

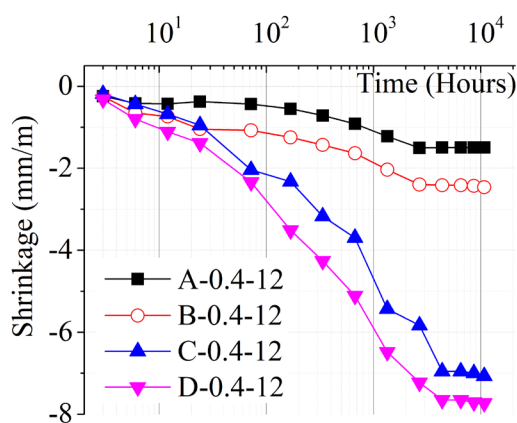


Fig. 13 Effect of SCBA on shrinkage

until 182 days, reaching final values of 7.07 mm/m and 7.72 mm/m, respectively – approximately 4.7 to 5.2 times higher than Group A. Minor shrinkage fluctuations may be associated with non-uniform moisture redistribution and internal evaporation during curing [36].

This increase is attributed to the high porosity of SCBA, which enables greater water absorption during mixing. Water loss during curing leads to higher volumetric contraction and shrinkage [23]. XRD results also revealed high crystalline silica content, which are less reactive and reduce geopolymer gel formation, resulting in a more shrinkage-prone matrix [22]. Furthermore, unburned carbon in SCBA, verified by EDX, can absorb activator solution, diminishing reaction efficiency. This unburned carbon also facilitates carbonation shrinkage, weakening bonding between particles [36]. The prolonged shrinkage period in high-SCBA samples aligns with findings by Rihan et al., where shrinkage stabilization occurred after 180 days in SCBA-based systems [24].

While many studies confirm the shrinkage-inducing effect of SCBA, some discrepancies exist. Le et al. reported that in slag-based systems, 10% SCBA reduced shrinkage by 15% due to enhanced matrix densification from SCBA-slag synergy [20]. In contrast, in the current fly ash-based system, low SCBA reactivity and high porosity dominate, leading to shrinkage increase – especially beyond 20% replacement. These discrepancies emphasize the importance of precursor type, SCBA fineness, and activator chemistry in shrinkage control.

#### 3.4.2 Effect of NaOH concentration on shrinkage

Fig. 14 illustrates the shrinkage behavior of geopolymer samples incorporating 10% sugarcane bagasse ash (SCBA) at NaOH concentrations of 8M, 12M, and 16M over 450

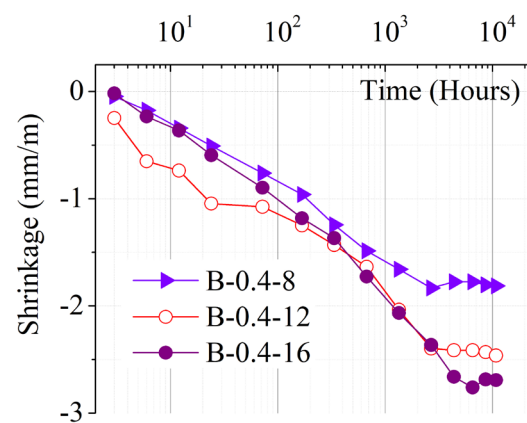


Fig. 14 Effect of NaOH concentration on shrinkage

days. Shrinkage increased slightly with higher NaOH concentration, with final values of 1.81 mm/m (8M), 2.46 mm/m (12M), and 2.69 mm/m (16M). During the initial stage (1-100 hours), all samples exhibited similar trends. After 112 days, shrinkage stabilized for the 8M and 12M samples, while the 16M sample continued to shrink until approximately 182 days [24].

This extended shrinkage duration may result from continued aluminosilicate dissolution under high alkali conditions, which delays structural densification and prolongs water release from the gel matrix [36]. Although the shrinkage increase was modest, the slower stabilization at 16M suggests that NaOH concentration influences long-term dimensional changes [25].

These findings align with results from Mermerdaş et al., which indicated that higher NaOH concentrations increase pore connectivity and moisture evaporation, thereby enhancing shrinkage in alkali-activated systems [37]. A similar conclusion was reached by Hanumananaik and Subramaniam, who reported that intensified reactions under high NaOH conditions lead to heterogeneous microstructures and non-uniform shrinkage behavior [38].

In contrast, Chen et al. observed significant shrinkage increases in GGBFS-metakaolin geopolymers when NaOH concentration exceeded 10M, highlighting the role of precursor composition [39]. The relatively moderate shrinkage differences observed in this study may be attributed to the porous structure of SCBA, which enhances internal moisture retention and moderates evaporation-induced shrinkage [23].

Compared to fly ash-only geopolymers, where NaOH concentration strongly affects both early and long-term shrinkage due to the high availability of amorphous aluminosilicates [16, 18], SCBA-FA systems tend to exhibit more stable shrinkage development. This behavior may result from the lower reactivity and higher porosity of SCBA, which buffers the effects of excessive alkali on microstructural contraction.

### 3.4.3 Effect of L/S ratio on shrinkage

Fig. 15 illustrates the shrinkage behavior of geopolymer pastes containing 10% sugarcane bagasse ash (SCBA) at L/S ratios of 0.2, 0.4, and 0.6 under a fixed NaOH concentration of 12M. After 450 days, final shrinkage values reached 0.24 mm/m, 2.46 mm/m, and 2.20 mm/m for L/S = 0.2, 0.4, and 0.6, respectively. Lower shrinkage and earlier stabilization were observed at L/S = 0.2, while higher L/S ratios exhibited greater and prolonged shrinkage.

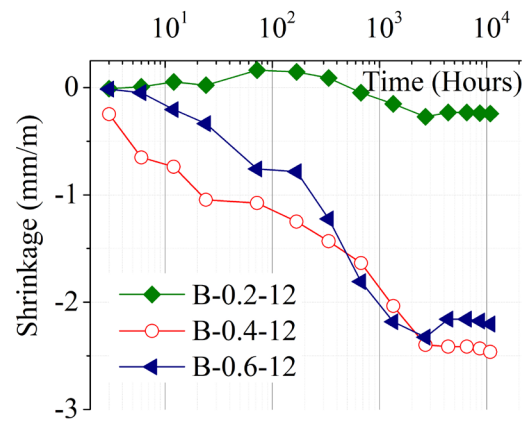


Fig. 15 Effect of L/S ratio on shrinkage

This trend aligns with previous studies reporting that increasing the L/S ratio leads to higher pore connectivity and greater moisture loss, which intensifies capillary tension and shrinkage development [17, 18]. Ling et al. demonstrated that higher water content accelerates evaporation and increases shrinkage unless shrinkage-reducing admixtures are applied [40]. Zhang et al. reported that nano-clay incorporation could mitigate shrinkage under high L/S conditions by refining pore structure and reducing free water pathways [36].

Although L/S = 0.6 exhibited slightly lower final shrinkage than L/S = 0.4, the stabilization period extended to 182 days, compared to 112 days at L/S = 0.4. This prolonged shrinkage may result from delayed internal structural rearrangement due to excess liquid, consistent with observations by Hanumananaik and Subramaniam regarding gel-phase heterogeneity under high liquid content [38]. Xu et al. further confirmed that low solid-to-liquid ratios promote shrinkage due to reduced gel densification and increased capillary stress [41].

Compared to fly ash-based geopolymers, FA-SCBA systems exhibit slightly lower early shrinkage at high L/S ratios, possibly due to SCBA's porous structure acting as internal curing reservoirs. However, this same porosity may prolong moisture migration and delay shrinkage stabilization. Teng et al. reported that fly ash-based mixes show sharper shrinkage peaks under high L/S, while SCBA-containing systems develop shrinkage more gradually [18].

### 3.5 SEM analysis

Fig. 16 presents SEM images of two geopolymer samples: B-0.4-12, which exhibited the highest compressive strength, and D-0.2-8, which exhibited the lowest compressive strength. The differences observed in these images reflect

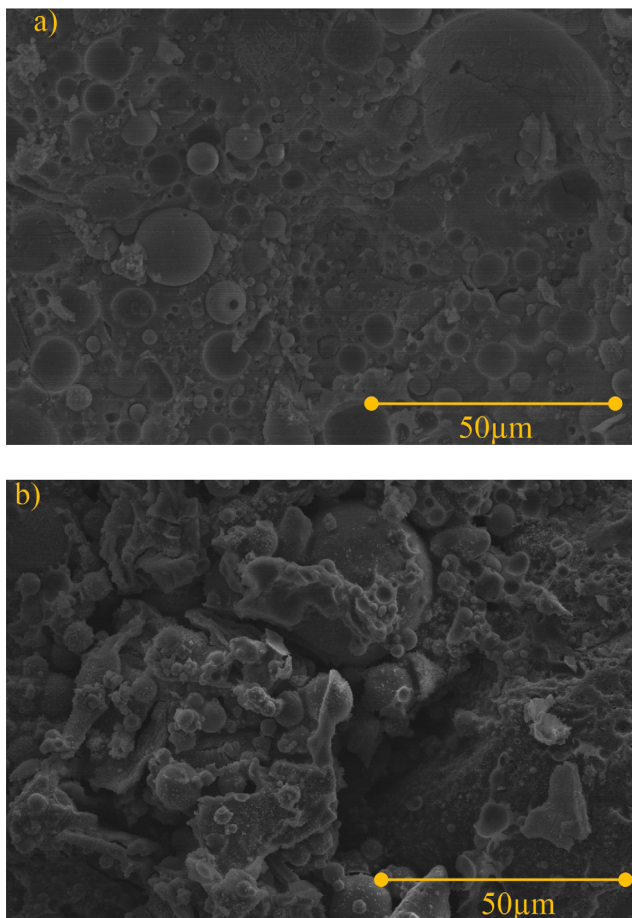


Fig. 16 SEM images, (a) B-0.4-12, (b) D-0.2-8

variations in matrix densification, the presence of unreacted particles, and the connectivity between solid phases.

Fig. 16(a) shows that the B-0.4-12 sample has a dense and homogeneous matrix, with a minimal presence of unreacted particles. No significant cracks are observed on the surface, and the geopolymer network appears well-connected, with no large voids between solid phases. This observation correlates with the high compressive strength (47.65 MPa), lowest apparent porosity (4.78%), and lowest water absorption (2.12%), indicating a well-developed microstructure formed during the geopolymerization process.

In contrast, Fig. 16(b) reveals that the D-0.2-8 sample has a loosely packed matrix, a high number of unreacted particles, and large voids between solid phases. Some microcracks and micropores are visible in the matrix, suggesting a weaker interconnectivity compared to B-0.4-12. These observed characteristics correlate with the low compressive strength (9.87 MPa), highest apparent porosity (19.90%), and highest water absorption (10.63%), suggesting incomplete geopolymerization and a non-homogeneous structure.

From these SEM observations, it is evident that samples with a denser structure and fewer unreacted particles

tend to achieve higher compressive strength and lower porosity. Conversely, samples with a loosely packed matrix, a high number of unreacted particles, and microcracks tend to exhibit lower strength, higher porosity, and greater water absorption.

#### 4 Conclusions

The principal conclusions of this study are summarized as follows:

A replacement of FA by sugarcane bagasse ash (SCBA) up to 10% under NaOH 12M and L/S = 0.4 resulted in the highest 90-day compressive strength (47.65 MPa), accompanied by the lowest water absorption (3.15%) and apparent porosity (4.78%). Increasing SCBA to 20% and 30% led to significant decreases in compressive strength (up to 36%) and bulk density (from 2.18 g/cm<sup>3</sup> to 1.49 g/cm<sup>3</sup>), with corresponding increases in porosity (up to 19.90%) and water absorption (up to 7.09%).

Compressive strength development was slower in SCBA-containing samples during the early stage but improved at later ages. A 30% SCBA replacement increased 90-day strength by 15% compared to 28-day strength, indicating late geopolymerization activity.

Shrinkage increased significantly with SCBA content. At 30% SCBA, shrinkage reached 7.72 mm/m, approximately 5.2 times higher than the control, with stabilization delayed until 182 days. This behavior was associated with the porous structure, crystalline silica, and unburned carbon in SCBA, contributing to reduced compressive strength and increased shrinkage.

NaOH concentration significantly affected compressive strength. An increase from 8M to 12M enhanced strength across all SCBA levels. Further increases to 16M had minimal or adverse effects depending on SCBA content. NaOH 12M was optimal for compressive strength and shrinkage control.

Shrinkage marginally increased with NaOH concentration (from 1.81 mm/m at 8M to 2.69 mm/m at 16M). Extended shrinkage periods at 16M were attributed to continued reaction and water migration.

Increasing L/S ratio from 0.2 to 0.4 significantly improved compressive strength, while increasing to 0.6 had minor effects. Shrinkage increased with L/S, especially at 0.6, due to higher water content and pore connectivity.

SEM observations confirmed that high-strength samples exhibited dense, crack-free matrices, while low-strength samples displayed high porosity and unreacted particles. XRD and EDX analyses showed SCBA contains

crystalline SiO<sub>2</sub> and residual carbon, contributing to reduced compressive strength and increased shrinkage.

SCBA presents potential as a partial FA replacement in sustainable geopolymer production. Optimal performance

was achieved at 10% SCBA, NaOH 12M, and L/S = 0.4. Applications in concrete require further investigation, particularly in terms of durability and long-term performance.

## References

- [1] Petrova, V. "Innovations in Cement Production: The Road to Sustainability and A Circular Economy", *The Eurasia Proceedings of Science Technology Engineering and Mathematics*, 29, pp. 295–303, 2024.  
<https://doi.org/10.55549/epstem.1573538>
- [2] Jaganmohan, M. "Major countries in worldwide cement production in 2024", [online] Available at: <https://www.statista.com/statistics/267364/world-cement-production-by-country/> [Accessed: 20 March 2025]
- [3] Bildirici, M. E., Ersin, Ö. Ö. "Cement production and CO<sub>2</sub> emission cycles in the USA: evidence from MS-ARDL and MS-VARDL causality methods with century-long data", *Environmental Science and Pollution Research*, 31(24), pp. 35369–35395, 2024.  
<https://doi.org/10.1007/s11356-024-33489-2>
- [4] Davidovits, J. "Geopolymer Chemistry and Applications", Institut Géopolymère, 2008. ISBN: 9782951482050
- [5] Duxson, P., Provis, J. L., Lukey, G. C., van Deventer, J. S. J. "The role of inorganic polymer technology in the development of 'green concrete'", *Cement and Concrete Research*, 37(12), pp. 1590–1597, 2007.  
<https://doi.org/10.1016/j.cemconres.2007.08.018>
- [6] Provis, J. L., van Deventer, J. S. J. "Geopolymers: Structures, processing, properties and industrial applications", Woodhead Publishing, 2009. ISBN: 978-1845694494
- [7] Xu, H., van Deventer, J. S. J. "The geopolymerisation of aluminosilicate minerals", *International Journal of Mineral Processing*, 59(3), pp. 247–266, 2000.  
[https://doi.org/10.1016/S0301-7516\(99\)00074-5](https://doi.org/10.1016/S0301-7516(99)00074-5)
- [8] Khale, D., Chaudhary, R. "Mechanism of geopolymerization and factors influencing its development: a review", *Journal of Materials Science*, 42(3), pp. 729–746, 2007.  
<https://doi.org/10.1007/s10853-006-0401-4>
- [9] Görhan, G., Danishyar, F. "The Effect of Silicate Modulus on the Properties of Polypropylene Fiber-reinforced Geopolymer Composite Material", *Periodica Polytechnica Civil Engineering*, 66(3), pp. 891–899, 2022.  
<https://doi.org/10.3311/PPci.19417>
- [10] Abdalla, T. A., Hussein, A. A. E., Ahmed, Y. H., Semmana, O. "Strength, durability, and microstructure properties of concrete containing bagasse ash – A review of 15 years of perspectives, progress and future insights", *Results in Engineering*, 21, 101764, 2024.  
<https://doi.org/10.1016/j.rineng.2024.101764>
- [11] Rehman, S. K. U., Imtiaz, L., Aslam, F., Khan, M. K., Haseeb, M., Javed, M. F., Alyousef, R., Alabduljabbar, H. "Experimental Investigation of NaOH and KOH Mixture in SCBA-Based Geopolymer Cement Composite", *Materials*, 13(15), 3437, 2020.  
<https://doi.org/10.3390/ma13153437>
- [12] Shee-Ween, O., Cheng-Yong, H., Abdullah, M. M. A. B., Wan-En, O., Yong-Jie, H., Hoe-Woon, T., Jia-Ni, L. "Effect of NaOH solution on mechanical properties and morphology of fly ash based cold-pressed geopolymer", *Archives of Metallurgy Materials*, 69, pp. 1353–1357, 2024.  
<https://doi.org/10.24425/amm.2024.151399>
- [13] Vigneshkumar, A., Christy, C. F., Muthukannan, M., Alengaram, J. "Fresh, hardened properties and microstructural analysis on the effect of NaOH molarities of industrial by-products based self-compacting geopolymer concrete", *International Review of Applied Sciences Engineering*, 2024.  
<https://doi.org/10.1556/1848.2024.00867>
- [14] Ghafoor, M. T., Ali, S., Imran, M., Saeed, M. "Impact of NaOH molarity on mechanical properties of fly ash slag based geopolymer concrete", *Proceedings of the Institution of Civil Engineers - Structures and Buildings*, 178(4), pp. 402–411, 2025.  
<https://doi.org/10.1680/jstbu.24.00169>
- [15] Vignesh, K., Rajkumar, D. "Investigation on the Effect of Concentration of NaOH with Partial Replacement of Fine Aggregate in Polyurethane-Foamed Geopolymer Concrete", *International Journal of Civil Engineering*, 11(12), pp. 117–128, 2024.  
<https://doi.org/10.14445/23488352/IJCE-V11I12P111>
- [16] Fernández-Jiménez, A., Palomo, A., Criado, M. "Microstructure development of alkali-activated fly ash cement: A descriptive model", *Cement and Concrete Research*, 35(6), pp. 1204–1209, 2005.  
<https://doi.org/10.1016/j.cemconres.2004.08.021>
- [17] Marczyk, J., Ziejewska, C., Plawecka, K., Bąk, A., Łach, M., Korniejewski, K., Hager, I., Mikuła, J., Lin, W.-T., Hebda, M. "Optimizing the L/S Ratio in Geopolymers for the Production of Large-Size Elements with 3D Printing Technology", *Materials*, 15(9), 3362, 2022.  
<https://doi.org/10.3390/ma15093362>
- [18] Teng, N. H., Yong, H. C., Abdullah, M. M. A., Yong-Sing, N., Hussin, K. "The physical and mechanical properties of fly ash geopolymers with various S/L ratios", In: *Proceedings of Advanced Material, Engineering & Technology*, Seoul, South Korea, 2020, 020026.  
<https://doi.org/10.1063/5.0023108>
- [19] Aliabdo, A. A., Abd Elmoaty, M., Salem, H. A. "Effect of water addition, plasticizer and alkaline solution constitution on fly ash based geopolymer concrete performance", *Construction and Building Materials*, 121, pp. 694–703, 2016.  
<https://doi.org/10.1016/j.conbuildmat.2016.06.062>
- [20] Le, D.-H., Sheen, Y.-N., Lam, M. N. T. "Potential utilization of sugarcane bagasse ash for developing alkali-activated materials", *Journal of Sustainable Cement-Based Materials*, 11(3), pp. 199–209, 2021.  
<https://doi.org/10.21650373.2021.1920513>

- [21] Rihan, M., Onchiri, R. O., Gathimba, N., Sabuni, B. "Effect of sugarcane bagasse ash addition and curing temperature on the mechanical properties and microstructure of fly ash-based geopolymer concrete", *Open Ceramics*, 19, 100616, 2024. <https://doi.org/10.1016/j.oceram.2024.100616>
- [22] Ahmad, W., Ahmad, A., Ostrowsky, K. A., Aslam, F., Joyklad, P., Zajdel, P. "Sustainable approach of using sugarcane bagasse ash in cement-based composites: A systematic review", *Case Studies in Construction Materials*, 15, e00698, 2021. <https://doi.org/10.1016/j.cscm.2021.e00698>
- [23] Sâmara, F., Figueiredo, P. F., Sousa, L. N., de Moura Solar Silva, M. V., Ribeiro Borges, P. H., da Silva Bezerra, A. C. "Reaction mechanisms in geopolymers produced from sugarcane bagasse ash", *Construction and Building Materials*, 377, 131124, 2023. <https://doi.org/10.1016/j.conbuildmat.2023.131124>
- [24] Rihan, M. A. M., Onchiri, R. O., Gathimba N., Sabuni, B. "Mechanical and Microstructural Properties of Geopolymer Concrete Containing Fly Ash and Sugarcane Bagasse Ash", *Civil Engineering Journal*, 10(4), pp. 1292–1309, 2024. <https://doi.org/10.28991/CEJ-2024-010-04-018>
- [25] Somna, R., Khamput, P., Somna, K. "Geopolymer Paving Blocks Made From Fly Ash and Bagasse Ash Under Different Curing Conditions", *Chiang Mai Journal of Science*, 51(3), e2024041, 2024. <https://doi.org/10.12982/CMJS.2024.041>
- [26] Chuewangkam, N., Nachaithong, T., Chanlek, N., Thongbai, P., Pinitsoontorn, S. "Mechanical and Dielectric Properties of Fly Ash Geopolymer/Sugarcane Bagasse Ash Composites", *Polymers*, 14(6), 1140, 2022. <https://doi.org/10.3390/polym14061140>
- [27] ASTM "ASTM C642-21 Standard Test Method for Density, Absorption, and Voids in Hardened Concrete", ASTM International, West Conshohocken, PA, USA, 2021. <https://doi.org/10.1520/C0642-21>
- [28] ASTM "ASTM C109/C109M-20 Standard test method for compressive strength of hydraulic cement mortars (using 2-in. or (50-mm) cube specimens)", ASTM International, West Conshohocken, PA, USA, 2020. [https://doi.org/10.1520/C0109\\_C0109M-20](https://doi.org/10.1520/C0109_C0109M-20)
- [29] ASTM "ASTM C596-23 Standard Test Method for Drying Shrinkage of Mortar Containing Hydraulic Cement", ASTM International, West Conshohocken, PA, USA, 2023. <https://doi.org/10.1520/C0596-23>
- [30] Bruker. "SPECTRA.ELEMENTS Software, (Version 4)", [computer program] Available at: <https://www.bruker.com/en/products-and-solutions/elemental-analyzers/xrf-spectrometers/xrf-software.html> [Accessed: 03 June 2025]
- [31] ACI "ACI Committee 116, ACI 116R-00 Cement and concrete terminology", American Concrete Institute, Farmington Hills, MI, USA, 2000.
- [32] ASTM "ASTM C618-22 Standard Specification for Coal Ash and Raw or Calcined Natural Pozzolan for Use in Concrete", ASTM International, West Conshohocken, PA, USA, 2023. <https://doi.org/10.1520/C0618-22>
- [33] Horiba Ltd. "EMAX-Analyser Software", [online] Available at: <https://www.horiba.com/int/scientific/technologies/energy-dispersive-x-ray-fluorescence-ed-xrf/what-is-x-ray-fluorescence-xrf/> [Accessed: 03 June 2025]
- [34] Luga, E., Peqini, K. "The The Influence of Oxide Content on the Properties of Fly Ash/Slag Geopolymer Mortars Activated with NaOH", *Periodica Polytechnica Civil Engineering*, 63(4), pp. 1217–1224, 2019. <https://doi.org/10.3311/PPci.14381>
- [35] Ahmer, A. S., Rashidah, M. H., Rashid, S., Muhammad, M. "Effect of particle size of fly ash and solid to liquid ratio on microstructure and mechanical properties of geopolymer", *Sustainable Processes Clean Energy Transition: ICSuPCET*, 29, pp. 152–159, 2023. <https://doi.org/10.21741/9781644902516-19>
- [36] Zhang, Y., Zhou, C., Song, J., Li, J., Gong, Y. "Foundry waste reutilization: Anti-shrinkage geopolymer based on nano-clay and coal gangue", *Construction and Building Materials*, 434, 136710, 2024. <https://doi.org/10.1016/j.conbuildmat.2024.136710>
- [37] Mermerdaş, K., Algin, Z., Ekmen, Ş. "Experimental assessment and optimization of mix parameters of fly ash-based lightweight geopolymer mortar with respect to shrinkage and strength", *Journal of Building Engineering*, 31, 101351, 2020. <https://doi.org/10.1016/j.jobe.2020.101351>
- [38] Hanumananaik, M. Subramaniam, K. V. L. "Shrinkage in low-calcium fly ash geopolymers for precast applications: Reaction product content and pore structure under drying conditions", *Journal of Building Engineering*, 78, 107583, 2023. <https://doi.org/10.1016/j.jobe.2023.107583>
- [39] Chen, Y.-C., Lee, W.-H., Cheng, T.-W., Li, Y.-F. "A Study on the Shrinkage and Compressive Strength of GGBFS and Metakaolin Base Geopolymer under Different NaOH Concentrations", *Materials*, 17(5), 1181, 2024. <https://doi.org/10.3390/ma17051181>
- [40] Ling, Y., Wang, K., Fu, C. "Shrinkage behavior of fly ash based geopolymer pastes with and without shrinkage reducing admixture", *Cement and Concrete Composites*, 98, pp. 74–82, 2019. <https://doi.org/10.1016/j.cemconcomp.2019.02.007>
- [41] Xu, Z., Yue, J., Pang, G., Li, R., Zhang, P., Xu, S. "Influence of the Activator Concentration and Solid/Liquid Ratio on the Strength and Shrinkage Characteristics of Alkali-Activated Slag Geopolymer Pastes", *Advances in Civil Engineering*, 2021(1), 6631316, 2021. <https://doi.org/10.1155/2021/6631316>